Chemistry–A European Journal
Full Paper
doi.org/10.1002/chem.202102743

Chemistry Europe
European Chemical Societies Publishing

Designing a Red-Emitting Viscosity-Sensitive BODIPY Fluorophore for Intracellular Viscosity Imaging

Karolina Maleckaitė,[a] Jelena Dodonova,[b] Stepas Toliautas,[c] Rugilė Žilėnaitė,[a] Džiugas Jurgutis,[d] Vitalijus Karabanovas,[d, e] Sigitas Tumkevičius,[b] and Aurimas Vyšniauskas*[a]

Abstract: Viscosity imaging at a microscopic scale can provide important information about biosystems, including the development of serious illnesses. Microviscosity imaging is achievable with viscosity-sensitive fluorophores, the most popular of which are based on the BODIPY group. However, most of the BODIPY probes fluoresce green light, whereas the red luminescence is desired for the imaging of biological samples. Designing a new viscosity probe with suitable spectroscopic properties is a challenging task because it is difficult to preserve viscosity sensitivity after modifying the molecular structure. Here we describe how we developed a new red-emitting, viscosity-sensitive, BODIPY fluorophore BP-PH-2M-NO_2 that is suitable for reliable intracellular viscosity imaging of lipid droplets in MCF-7 breast cancer cells. The design of BP-PH-2M-NO_2 was aided by DFT calculations that allowed a successful prediction of the viscosity sensitivity of fluorophores before synthesis. In summary, we report a new red viscosity probe possessing monoexponential fluorescence decay that makes it attractive for lifetime-based viscosity imaging.

Introduction

Imaging microviscosity, a bulk viscosity equivalent on a microscopic scale, can provide important information about the diffusion-controlled processes in biosystems. Determination of microviscosity can help to indicate the development of atherosclerosis,[1] diabetes,[2] and Alzheimer's disease.[3] Viscosity-sensitive fluorophores, called 'molecular rotors', provide one of the easiest methods to image microviscosity.[4] The mechanism of molecular rotors is based on a change in fluorescence signal that arises from the competition between fluorescence and intramolecular rotation, with the latter leading to faster non-radiative relaxation.[5–8] A high-viscosity environment restricts the rotation and results in the long stay of the molecule in a fluorescent state, leading to higher fluorescence intensity and longer fluorescence lifetime.[5,9,10] The fluorescence lifetime is not affected by the fluorophore concentration, which makes the lifetime-based molecular rotors more advantageous than simple fluorescence intensity probes.[11–13] Lifetime-based molecular rotors are compatible with Fluorescence Lifetime Imaging Microscopy (FLIM) which can record a time-resolved fluorescence decay in every pixel of the image, providing a convenient method for viscosity-imaging.[12–15]

The most widely used viscosity-sensitive molecular rotors are BODIPY-C_{10} and BODIPY-C_{12} (Figure 1) which differ only in the length of the hydrocarbon chain and have otherwise identical photophysical properties.[12,16] BODIPY-C_{10} and other closely related fluorophores have been used to measure microviscosity in live cells,[12,17] plasma membranes,[18–20] collagen in tumor tissues,[21] eye lens cell membranes,[22] mitochondria,[13] model lipid membranes,[23–26] lipid microbubbles,[27] polymers[28]

[a] K. Maleckaitė, R. Žilėnaitė, Dr. A. Vyšniauskas
Center of Physical Sciences and Technology Saulėtekio av. 3, Vilnius, LT-10257, Lithuania
E-mail: aurimas.vysniauskas@ftmc.lt

[b] Dr. J. Dodonova, Prof. S. Tumkevičius
Institute of Chemistry, Faculty of Chemistry and Geosciences, Vilnius University Naugarduko str. 24, Vilnius, LT-03225, Lithuania

[c] Dr. S. Toliautas
Institute of Chemical Physics, Faculty of Physics, Vilnius University Saulėtekio av. 9-III, Vilnius, LT-10222, Lithuania

[d] D. Jurgutis, Prof. V. Karabanovas
Biomedical Physics Laboratory, National Cancer Institute
P. Baublio str. 3b, Vilnius, LT-08406, Lithuania

[e] Prof. V. Karabanovas
Department of Chemistry and Bioengineering,
Vilnius Gediminas Technical University
Saulėtekio av. 11, Vilnius, LT-10223, Lithuania

Supporting information for this article is available on the WWW under https://doi.org/10.1002/chem.202102743

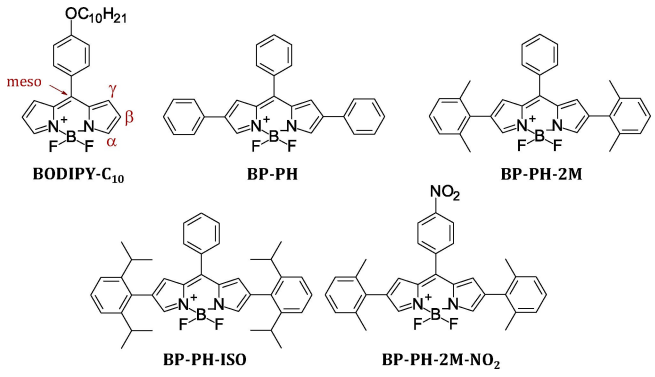

Figure 1. The structures of the most widely used molecular rotor BODIPY-C_{10} together with new fluorophores explored in this work. The red-coloured notes indicate the substituted position of the BODIPY core.

and aerosols.[29] The main advantage of BODIPY-C_{10}/C_{12} is a monoexponential fluorescence decay, which simplifies the data analysis and enables a quicker recording of the lifetime-based viscosity map using FLIM.[30] The greatest drawback of BODIPY-C_{10}/C_{12} is green-light absorbance and fluorescence wavelengths, around 500 nm, which are rather short if imaging of the biological sample is desired. One must red-shift the fluorophore's spectra to fall into the tissue optical window (650–1350 nm), where the light penetration is deeper and there is a minimal overlap with autofluorescence and fluorescence of widely used probes, such as green fluorescent protein (GFP).[31] Red fluorescence wavelengths can be achieved simply by introducing conjugated substituents and extending the conjugation length within the fluorophore.[32,33] However, the difficult part is to ensure that the new modified red-emitting BODIPY probe remains sensitive to viscosity. There is little known about how fluorophore's structure is related to its viscosity sensitivity[4] and therefore it is extremely difficult to predict if a proposed fluorophore will be a molecular rotor. In such case, the only remaining option is a synthesis of a large number of fluorophores with various modifications, which is a time-consuming endeavour with a low probability of success. In this research, we show how quantum chemical calculations can help to determine viscosity-sensitive properties of the conjugate before its synthesis and then use them for developing a red BODIPY viscosity probe. First, we predict that a BODIPY molecular rotor with merely extended conjugation is unlikely to be viscosity-sensitive but then we show how this can be counteracted by further modifications. Second, we proceed to synthesise and characterise new BODIPY fluorophores (Figure 1) that we previously examined theoretically and demonstrate that our predictions made using density functional theory (DFT) results are largely correct. As a result, we have a new BODIPY viscosity probe with a significantly red-shifted emission that is capable of reliable intracellular viscosity imaging.

Results and Discussion

Fluorophore design

To achieve longer absorbance and fluorescence wavelengths than the ones of BODIPY-C_{10}, the conjugation of the molecular structure has to be extended.[34–36] It is known that the modification of the substituent in the *meso* position barely changes the absorption and emission spectrum due to a weak conjugation with the BODIPY core.[37] Moreover, any substituent in the γ position of the BODIPY core, next to the phenyl ring, eliminates the viscosity sensitivity[38] with one notable exception.[39] In contrast, the introduction of substituents into the α position is a more viable option, although it has been shown that methyl groups in the α position reduce the viscosity sensitivity.[38]

Therefore, the best option to redshift the spectra of BODIPY-C_{10} while preserving viscosity sensitivity seems to be the introduction of conjugated substituents into the β position. We chose to use phenyl groups (Figure 1).

DFT calculations

To predict the absorption, fluorescence wavelengths, the viscosity sensitivity of the proposed molecules (Figure 1) and to select the most promising molecules for synthesis, the quantum chemical calculations were performed. Theoretical calculations showed that the extension of the conjugated system should successfully shift absorption and fluorescence spectra to the longer wavelengths (Table 1). The overestimation of electronic transition energies in BODIPYs by DFT is a well-known problem. Nevertheless, DFT provides accurate relative energies and allows comparison between different fluorophores even if the absolute energy values are incorrect.[40–42]

The previous work by Toliautas et al.[43] and Liu et al.[38] has demonstrated that the viscosity sensitivity of BODIPY molecular rotors is determined by the activation energy barrier the fluorophore needs to cross during the non-radiative relaxation (Figure 2A). Immediately upon excitation the BODIPY fluorophore reaches the fluorescent state at local minimum ($S_{1,m}$, Figure 2B), where the rotation angle θ is approximately 45°. However, the fluorophore can cross a relatively small energy barrier, go through a transition state (TS, Figure 2B), and reach another minimum at 0° angle (labeled $S_{1,r}$, Figure 2B). The rotation is followed by the loss of planarity, with the BODIPY core becoming V-shaped (Figure 2C).[43,44] From $S_{1,r}$ the molecule can rapidly relax to the ground state non-radiatively.[43,45–48] The $S_{1,m}$ to $S_{1,r}$ transition rate is heavily viscosity-dependent.[38] Therefore, if the transition rate is slow due to the high energy barrier, other relaxation pathways will dominate, which will render the fluorophore viscosity-insensitive.

To estimate the viscosity sensitivity of the proposed molecules, we have calculated how the energy of the S_1 state depends on the dihedral angle between the phenyl ring in the *meso* position and the BODIPY core. Figure 2B compares the potential energy surface (PES) of the fluorophores in the excited

Table 1. Theoretical ($_t$) and experimental ($_e$) values of absorption (λ_A) and fluorescence emission maxima (λ_F), Stokes shifts ($\bar{\nu}_{SS}$), fluorescence quantum yields (QY), and molar extinction coefficients (ε_e) for BP-PH, BP-PH-2M, BP-PH-2M-NO_2, BP-PH-ISO and BODIPY-C_{10} in toluene.

Derivative	λ_{tA} [nm]	λ_{tF} [nm]	λ_{eA} [nm]	λ_{eF} [nm]	$\bar{\nu}_{eSS}$ [cm^{-1}*]	QY_e [%]	ε_e [$M^{-1}\cdot cm^{-1}$]
BP-PH	485	535	590	630	1076	28	3.3×10^4
BP-PH-2M	451	511	530	585	1774	22	3.3×10^4
BP-PH-2M-NO_2	463	544	545	620	2220	4	6.5×10^4
BP-PH-ISO	448	490	535	575	1300	36	8×10^4
BODIPY-C_{10}	423	443	500	515	583	12	6.4×10^4

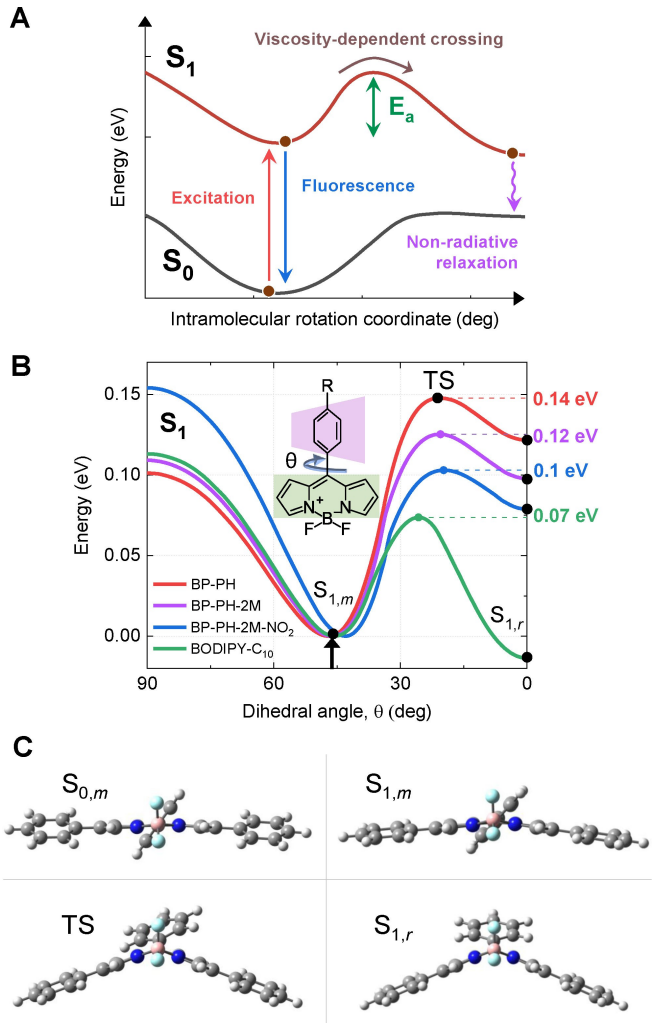

Figure 2. (A) Photophysical model explaining the viscosity-sensing mechanism of BODIPY probes. Upon excitation (red arrow) the molecule can return to the S_0 state through fluorescence (blue arrow) or by overcoming an activation energy barrier (E_a) followed by a non-radiative relaxation (pink arrow). (B) Potential energy surface (PES) curves of the first excited electronic state (S_1) of BP-PH (red), BP-PH-2M (purple), BP-PH-2M-NO_2 (blue), and BODIPY-C_{10} (green) calculated by TD-DFT. The PES curve of BP-PH-ISO is shown in Figure S3, Supporting Information due to the similarity to BP-PH-2M. The x-axis shows the dihedral angle θ between the BODIPY core and the *meso*-phenyl (inset). Fluorescence takes place in the vicinity of the minimum denoted $S_{1,m}$, whereas a fast non-radiative relaxation occurs via the minimum $S_{1,r}$. The energy of the local minimum $S_{1,m}$ at approximately 45° is set to 0 eV as a reference point for easier comparison. A value of the energy barrier for each molecule is shown on the right side of the graph. The black arrow indicates the dihedral angle immediately upon excitation. (C) Molecular structures of BP-PH at ground-state minimum $S_{0,m}$, excited-state minima $S_{1,m}$ and $S_{1,r}$, a transition state (TS) between the $S_{1,m}$ and $S_{1,r}$ .The geometries of BP-PH-2M and BP-PH-2M-NO_2 are closely similar to the ones of BP-PH.

state and reveals differences between the new molecules and the well studied BODIPY-C_{10}. The PES and the geometries of the new fluorophores (Figure 2C, the coordinates are provided in the Supporting Information) are consistent with the PES and geometries of the previously investigated *meso*-phenyl-BODIPYs.[43,45–48] Therefore, we consider that the main non-radiative relaxation pathway remains the same and involves the V-bending of the BODIPY core, as reported previously.[45–47]

The results show that attaching bare phenyl groups only (BP-PH) increases the energy barrier compared to BODIPY-C_{10} by approximately 70 meV. To estimate the decrease of viscosity-dependent relaxation rate due to the barrier increase, we used the following relationship [Eq. (1)]:

$$k_{nr}(\eta) \propto \exp\left(-\frac{E_a}{k_b T}\right) \quad (1)$$

where E_a is the activation energy barrier, k_b – Boltzmann's constant and T is a room temperature in kelvins. The Equation (1) shows that the estimated barrier increase (70 meV) should make the viscosity-sensitive non-radiative relaxation rate slower by a factor of 15 at room temperature. As a result, other relaxation pathways will dominate, making BP-PH barely sensitive to viscosity.

To investigate the reason behind the barrier increase upon introducing the phenyl groups, we have calculated the corresponding energy values of the artificial compound when the β-phenyls are rotated 90° out of conjugation. Upon the loss of conjugation, the energy barrier for non-radiative relaxation located between $S_{1,r}$ and $S_{1,m}$ greatly diminishes (Figure S1, Supporting Information) and becomes more similar to the one for BODIPY-C_{10}. This means that the higher barrier is caused by the conjugation of the new phenyl groups with the BODIPY core. Furthermore, this finding implies that shifting the spectra of BODIPY-C_{10} by extending its conjugation unavoidably leads to the loss of viscosity-sensitivity.

To deal with this problem, we have proposed two solutions. Firstly, we have attached steric moieties (methyl or isopropyl groups) to the β-phenyls, which forces the phenyl rings to partially rotate out of the BODIPY plane. This may help to reach the middle ground, where the spectral red shift is not as strong but the molecules are more sensitive to viscosity. Secondly, we have attached a nitro group, which has been previously shown to reduce the energy barrier.[43] The quantum chemical calculation results shown in Figure 2B demonstrate that introducing methyl groups reduces the energy barrier by 0.02 eV, whereas the nitro group leads to the reduction by yet another 0.02 eV. The final value of the energy barrier for BP-PH-2M-NO_2 (0.10 eV) is not far off the value for BODIPY-C_{10}, which allows us to expect that BP-PH-2M-NO_2 will be able to effectively sense the viscosity and at the same time emit at the higher wavelength than BODIPY-C_{10}. The shapes of the highest occupied (HOMO) and the lowest unoccupied molecular orbitals (LUMO) (Figure S2) reveal that the nitro group increases the electron density on the *meso*-phenyl ring and on the bond connecting the ring to the BODIPY core. Therefore, a better overlap of *p* orbitals is achieved upon intramolecular rotation, which leads to the reduction of the energy barrier.

Absorbance and fluorescence spectra

To verify our DFT-based predictions, we have synthesised the BODIPY fluorophores shown in Figure 1. As shown in Figure 3A, the absorption spectra of all dyes consist of the higher energy

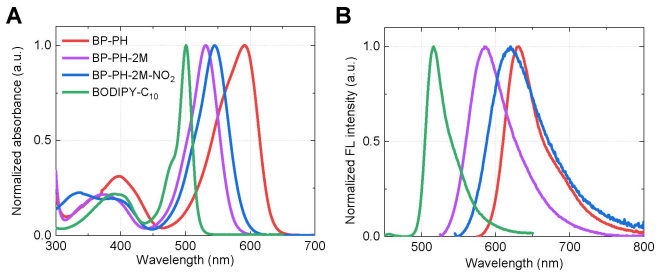

Figure 3. The absorption (A) and fluorescence (B) spectra of BP-PH (red), BP-PH-2M (purple), BP-PH-2M-NO_2 (blue), and BODIPY-C_{10} (green) obtained in toluene.

band at 300–400 nm and the main absorption band, which is located at 450–630 nm. The experimental spectra follow the trends predicted by theoretical calculations (Table 1) quite closely. As expected, the position of the main band of previously unreported derivatives has 20–90 nm longer wavelengths in contrast to well investigated BODIPY-C_{10}. BP-PH shows the largest shift to the longer wavelengths with the absorption peak at 590 nm. Methyl groups attached in both *ortho* positions on the benzene rings (BP-PH-2M) shift the absorption maximum to 530 nm due to the decrease in conjugation because methyl groups prohibit planarization of the β-phenyls. Increasing the steric hindrance by replacing the methyl groups with isopropyl groups (BP-PH-ISO) does not drastically shift the spectra (Figure S3A–B). The introduction of the NO_2 group (BP-PH-2M-NO_2) results in the absorption maximum at 545 nm. A similar effect was observed previously for BODIPY viscosity sensors with no substituents in the β positions.[43]

Similar red-shift tendencies are also seen in the fluorescence spectra (Figure 3B). BP-PH shows the largest bathochromic shift with the fluorescence peak at 630 nm due to the increased conjugation. Because of the steric hindrance, the fluorescence bands of BP-PH-2M and BP-PH-2M-NO_2 appear at shorter wavelengths, with the peaks at 585 nm and 620 nm, respectively. A Stokes shift for BP-PH and BP-PH-2M was 1076 cm^{-1} and 1774 cm^{-1}, respectively, while for the derivative with a nitro group it increased to 2220 cm^{-1}. Furthermore, we have determined the fluorescence quantum yields in toluene for all new derivatives (Table 1). As expected, the new derivatives with the higher energy barrier show larger quantum yields because the molecule stays longer in the fluorescent state before overcoming the potential energy barrier (Figure 2A). The fact that BP-PH-2M-NO_2 shows a smaller fluorescence quantum yield than BODIPY-C_{10} despite having the higher barrier may be the result of additional non-radiative relaxation pathways that are present in the new fluorophore.

Additionally, we performed the experiments in different polarity solvents (from non-polar to very polar: cyclohexane, toluene, chloroform, dichloromethane (DCM), dichloroethane (DCE), dimethyl sulfoxide (DMSO), methanol). The derivatives show no strong solvatochromism, resulting in the red-shift of 14, 16, 8 and 19 nm for BP-PH, BP-PH-2M, BP-PH-ISO, and BP-PH-2M-NO_2, respectively, when going from the least polar to the most polar solvents (Figure S4).

Influence of viscosity

Since our new BODIPY derivatives are hydrophobic, they are likely to localize in non-polar lipid bilayers during their application in live cell imaging. Due to this reason, non-polar toluene-castor oil mixtures were chosen for determining the viscosity sensitivity of the new fluorophores. Mixtures ranging from pure toluene to pure castor oil covering 0.5-920 cP viscosity range were used. The majority of fluorescence decays in mixtures were monoexponential, although some of the decays were biexponential owing to the small contribution from castor oil, which is itself fluorescent. Data shown in Figure 4A–C demonstrate time-resolved fluorescence decays at increasing viscosity for all new derivatives. The fluorescence lifetime values are shown in Figure 4D, exact lifetimes and amplitudes are shown in Table S2, Supporting Information. In the case of biexponential decays, intensity-weighted mean lifetimes are shown [Eq. (1)]. The experimental results closely follow our theoretical predictions; BP-PH has the weakest viscosity sensitivity out of all new BODIPY fluorophores. The introduction of methyl groups (Figure 4B) or isopropyl groups (Figure S3D) slightly increased viscosity sensitivity but to a lesser degree than required for an applicable viscosity sensor. However, the addition of the nitro group has resulted in a very

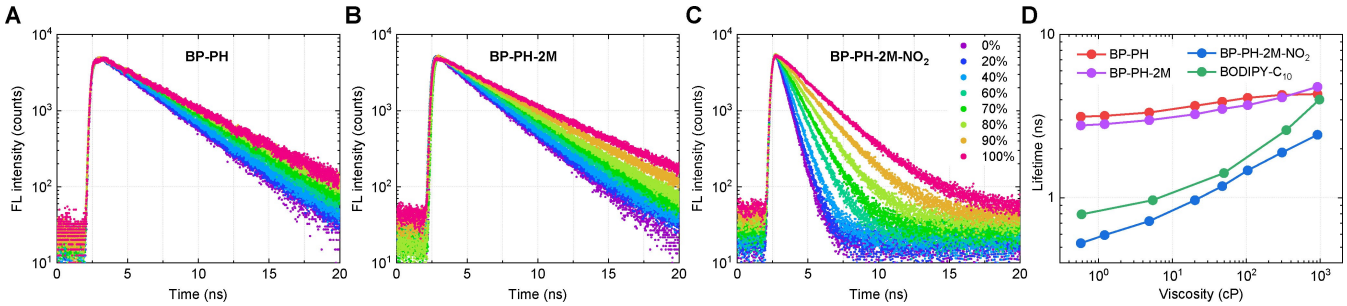

Figure 4. Time-resolved fluorescence decays of BP-PH (A), BP-PH-2M (B), BP-PH-2M-NO_2 (C) obtained in toluene-castor oil mixtures. The colours in the legend indicate the volume fraction of castor oil in the mixture. (D) Fluorescence lifetimes of BP-PH (red), BP-PH-2M (purple), BP-PH-2M-NO_2 (blue), and BODIPY-C_{10} (green) obtained in toluene-castor oil mixtures.

strong viscosity sensitivity, which is comparable to the sensitivity of the most applied BODIPY molecular rotor BODIPY-C_{10} (Figure 4D) as both molecules displayed similar *x* values for Förster-Hoffmann fits[5,49] (Figure S5). Additionally, the dynamic range of the probe, which can be calculated from the lifetime ratio at high and low viscosities, increased from 1.4 to 4.6, for the molecules BP-PH and BP-PH-2M-NO_2, respectively. This is supplemented by fluorescence intensities at low and high viscosities shown in Figure S6. The quantum yields of fluorescence of BP-PH-2M-NO_2 in toluene-castor oil mixtures are shown in Table S3, Supporting Information.

Furthermore, we proved that the nitro-substitution is a universal strategy for increasing the viscosity-sensitivity of BODIPY viscosity probes as it has now been shown to work with β-phenyl-substituted BODIPYs in addition to BODIPYs without substituents in the β position[43] (Figure S7).

The importance of this result is twofold. First, we managed to significantly increase the absorption and emission wavelength of BODIPY-C_{10}, which now is very close to the red region of the visible spectrum. Second, our discovered trend in viscosity sensitivity of new BODIPY derivatives matches the trend in the energy barrier heights (Figure 2A). This further supports the hypothesis that viscosity sensitivity is determined by the height of the energy barrier for non-radiative relaxation. This knowledge is crucial for being able to make predictions about viscosity sensitivity of proposed fluorophores by theoretical calculations.

The influence of temperature and solvent polarity on fluorescence lifetime was also investigated (Figure S8). All derivatives showed weak temperature sensitivity as demonstrated by decreasing fluorescence lifetimes in cyclohexane with increasing temperature (Figure S8A). Also, the values of the lifetimes for BP-PH and BP-PH-2M are comparable, while BP-PH-ISO showed around 1 ns longer lifetimes in cyclohexane. BP-PH-2M-NO_2 has much lower lifetimes due to fast non-radiative relaxation in a solvent of low viscosity. Very similar dependency is seen when the polarity of solvent is changed: lifetimes decrease with increasing polarity. BP-PH, BP-PH-2M and BP-PH-ISO demonstrate comparable lifetimes, while derivative with $-NO_2$ group showed lower lifetimes and less sensitivity to polarity (Figure S8B). These observations let us state that the viscosity sensitivity was drastically increased with an attachment of the $-NO_2$ group. This improvement lets viscosity sensitivity dominate over the observed sensitivities to temperature and solvent polarity.

Cellular imaging

The above-described results show that BP-PH-2M-NO_2 stands out of all the new derivatives, demonstrating strong viscosity sensitivity. We decided to use this conjugate for live cell imaging. MCF-7 breast cancer cells were stained using large unilamellar vesicles (LUV) containing BP-PH-2M-NO_2 incorporated into the lipid membrane of LUVs.

The fluorescence image of MCF-7 cells after staining (Figure 4A) revealed that BP-PH-2M-NO_2 successfully internalizes into the live cells. The granulated pattern of red fluorescence inside MCF-7 cells indicates that BP-PH-2M-NO_2 intensely stains spherical organelles. Further intracellular colocalisation analysis (Figures S10 and S11) showed accumulation of BP-PH-2M-NO_2 in lipid droplets. Recorded FLIM image (Figure 5B) showed monoexponential fluorescence decays (Figure S9A) with the mean lifetime of 1532 ps. Using this lifetime, toluene-castor oil calibration (Figure 4D) allowed us to assign a dynamic viscosity of 123 cP. Similar viscosity values were published in other articles, where BODIPY molecules were used to stain plasma and internal membranes of the live cells.[12,20,21]

The fluorescence spectrum of BP-PH-2M-NO_2 in live cells closely matched the spectrum in toluene both in terms of position and shape (Figure S9). Such spectral resemblance in addition to monoexponential decays demonstrated that the photophysical properties of the probe did not change when moving from toluene-castor oil mixtures to the complex intracellular environment. Therefore, toluene-castor oil mixtures are suitable solvents for calibrating BP-PH-2M-NO_2. Additionally, BP-PH-2M-NO_2 shows no signs of aggregation or degradation in the intracellular environment, as this would lead to change in the fluorescence spectrum and the emergence of an additional exponential component in the fluorescence decay. As a result, BP-PH-2M-NO_2 is suitable for staining live MCF-7 cells and reporting intracellular viscosity in lipid droplets. In the future work, we plan to modify the structure of BP-PH-2M-NO_2, so it could be directed to other cellular organelles besides lipid droplets.

Conclusions

To conclude, we have successfully designed and synthesised a red-emitting BODIPY viscosity probe BP-PH-2M-NO_2. The design process of BP-PH-2M-NO_2 was greatly aided by DFT calculations,

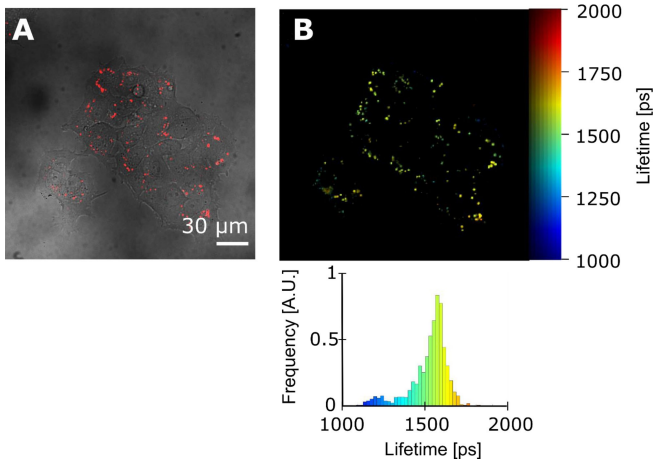

Figure 5. Live MCF-7 cells stained with BP-PH-2M-NO_2. (A) Brightfield image superimposed with a fluorescence image of BP-PH-2M-NO_2 showing the staining of lipid droplets. (B) FLIM image with the lifetime histogram at the bottom. The mean lifetime is 1532 ± 74 ps (one standard deviation). The fluorescence was excited at 560 ± 5 nm and detected over the range 621–755 nm.

which were used to obtain an energy barrier height that prevents viscosity-dependent non-radiative relaxation. This was used to predict the viscosity sensitivity of the target molecular structures before synthesis. To our knowledge, this is the first example in the literature where such an approach was used. The new fluorophore emits at a significantly longer wavelength and has a Stokes shift that is four times larger than the one of widely used green viscosity probe BODIPY-C_{10}/C_{12} and its variants. Furthermore, the new probe successfully senses viscosity in lipid droplets of live MCF-7 cells and shows a monoexponential fluorescence decay in a complex intracellular environment. Such a property is a highly desired feature as it enables reliable viscosity sensing via the FLIM technique. Overall, our work shows how DFT calculations can be exploited for the development of a new red fluorescent viscosity sensor with attractive properties.

Experimental Section

Dyes, reagents, and solvents

BODIPY-C_{10} was synthesised as previously reported.[12] The synthesis of novel BODIPY derivatives BP-PH, BP-PH-2M, BP-PH-ISO and BP-PH-2M-NO_2 was accomplished using Suzuki reaction of corresponding β-dibromo BODIPY derivatives with arylboronic acids in the presence of $Pd(OAc)_2$/SPhos as a catalyst system. The synthetic details and characterization data of the synthesized compounds are presented in Supporting Information. Stock solutions of all dyes were prepared in toluene at the concentration of 2–2.5 mM and diluted for further experiments in a solvent or solvent mixtures of interest. Toluene, castor oil, cyclohexane, chloroform, DCM, DCE, DMSO, ethanol (EtOH) and methanol (MeOH) were obtained from Sigma-Aldrich. The viscosities of toluene/castor oil mixtures at a variable temperature were measured by using a vibro viscometer (SV10, A&D).

Absorption, steady-state, time-resolved fluorescence, and quantum yield measurements

Absorption spectra were measured by using a Jasco V-670 spectrophotometer. Fluorescence spectra and time-resolved fluorescence were recorded with the Edinburgh-F900 (Edinburgh Instruments) fluorimeter. Excitation of the new molecules was performed by using the WhiteLase Micro (Fianium) laser together with bandpass filters (Thorlabs) with 10 nm bandwidth centred at 520 nm (BP-PH-2M and BP-PH-ISO), 540 nm (BP-PH-2M-NO_2), 570 nm (BP-PH), while previously reported BODIPY-C_{10} was excited using 1 MHz frequency picosecond pulsed diode laser EPL-470 (Edinburgh Instruments) emitting at 473 nm. Fluorescence decays were measured using the time-correlated singlephoton counting technique. Fluorescence decays had 5000 counts at the peak of the decay with 20 ns (BP-PH, BP-PH-2M, BP-PH- ISO and BP-PH-2M-NO_2) and 50 ns (BODIPY-C_{10}) window being used with 4096 channels. Quantum yields (QY) were determined by comparative method using Rhodamine-101 ($QY_F = 0.91$ in EtOH; used for BP-PH),[50] Rhodamine-6G ($QY_F = 0.94$ in EtOH; used for BP-PH-2M, BP-PH-2M, BP-PH-2M-NO_2, BP-PH-ISO),[50] and fluorescein ($QY_F = 0.95$ in 0.1 M $NaOH_{aq}$; used for BODIPY-C_{10})[51] as a standard. Quartz cuvettes (10 mm) were used for absorption, fluorescence, and QY measurements. The concentration of dyes was 2–8 μM.

Theoretical calculations

Structural and optical properties of the investigated molecular rotors were modelled by performing quantum chemical computations based on DFT,[52] as well as time-dependent DFT[53] for the excited state properties. M06-2X hybrid functional[54] and cc-pVDZ basis set for the electronic wave-function[55] were used in all stages of computations. The choice was based on the internal benchmarks and the findings of Momeni et al.[56] Coordinate scans of the potential energy surfaces (PES) of the first excited molecular state S_1 were constructed by performing relaxed geometry optimizations at the various fixed values of the rotation angle (*meso* position in Figure 1). The inclusion of zero-point vibrational energy (ZPVE) in estimation of the S_1 energy had an insignificant effect, changing relative shape of the surfaces by 6–7 meV (Table S1, Supporting Information). Bulk solvent effects on the solute molecules were taken into account by the conductor-like polarizable continuum model (C-PCM)[57] with solvent parameters of toluene. Even though PCM might have been sufficient, we used C-PCM in order to be consistent with our previous calculations.[16,43] Calculations were carried out using electronic structure modelling package Gaussian09.[58] Properties of BODIPY-C_{10} variant were obtained substituting its molecular structure with alkyl group shortened to a single carbon atom; this change was shown earlier to have no effect on the photophysical results,[16] while significantly reducing numerical calculation times.

Imaging of live cancer cells

Stock solutions of 1,2-dipalmitoyl-*sn*-glycero-3-phosphocholine (DPPC) used for LUVs were purchased from Avanti Polar Lipids. Phosphate-buffered saline (PBS) buffer was prepared using a well-known protocol.[59] NaCl, KCl, Na_2HPO_4 an KH_2PO_4 were purchased from CARL-ROTH. LUVs were prepared by the extrusion method. A 222 μL mixture of DPPC lipid and BP-PH-2M-NO_2 dye concentrate in chloroform was blow-dried using nitrogen. The dried solution was put in the desiccator and the remaining solvent evaporated under vacuum for 1 hour. After this, 2.4 mL PBS buffer was used for hydration of the dry lipid sample. The solution was vortexed and sonicated above the phase transition temperature (>41 °C). The solution was extruded 10 times through a polycarbonate membrane with a pore diameter of 0.1 μm using Avanti Polar Lipids Mini-Extruder. It was ensured that the process is carried out above the phase transition temperature.

Human breast cancer cell line MCF-7 was purchased from European Collection of Cell Cultures and cultured in cell growth medium (Dulbecco's modified Eagle's medium – DMEM), supplemented with 10% fetal bovine serum, 100 μg /mL penicillin and 100 μg/mL streptomycin (Gibco). Cells were maintained at 37 °C in 5% CO_2 and routinely subcultured 2–3 times a week in 25 cm^2 culture dishes. For live cell imaging, cells were seeded into an 8-chambered cover glass plate (Nunc, Lab-Tek) with a density of 3×10^4 cells/chamber and subsequently incubated at 37 °C in 5% CO_2 for 24 h. MCF-7 cells were treated with BP-PH-2M-NO_2 encapsulated in lipid vesicles in PBS for 15 min at 37 °C. After incubation, the cells were washed with Dulbecco's phosphate-buffered saline with Ca^{2+} and Mg^{2+}, w/o Phenol Red (DPBS) (Cegrogen Biotech). For BODIPY-h and Nile Red (Invitrogen) localisation, cells were stained with 9 μM BODIPY-h (stock solution prepared in DMSO and diluted with DPBS) for 60 min at 37 °C. Afterwards, cells were treated with 314 nM Nile Red (stock solution prepared in DMSO and diluted with DPBS) for 10 min at room temperature. For localisation of BP-PH-2M-NO_2 and BODIPY-h, MCF-7 cells were treated with BP-PH-2M-NO_2 encapsulated in lipid vesicles in PBS for 15 min at 37 °C. Afterwards, cells were incubated with 9 μM BODIPY-h for 60 min 37 °C. After each staining step, cells were washed 3 times with warm DPBS. During

the imaging, cells were maintained at 37 °C in the Microscope Stage Incubation System (OkoLab) in a humidified atmosphere containing 5% of CO_2 (0.80 Nl/min O_2 and 0.04 Nl/min CO_2). For localisation experiments, control samples were prepared for finding the detection parameters that eliminate emission bleed-through from Nile Red and BP-PH-2M-NO_2 in the green channel (501-590 nm), where the fluorescence of BODIPY-h was detected.

Samples were imaged using Nikon Eclipse Te2000-S, C1si confocal laser scanning microscope (Nikon) equipped with Fianium White-Lase Micro supercontinuum laser (NKT Photonics) with a pulse repetition rate of 30 MHz and filtered using 480/10 nm or 560/10 nm band-pass filters (Thorlabs Inc.). Imaging was performed using 60×/1.4 NA oil immersion objective (Nikon). The 32-channel spectral detector was applied to measure the fluorescence spectra of BP-PH-2M-NO_2 and BODIPY-h in live MCF-7 cells. FLIM imaging was performed using a Lifetime and Fluorescence Correlation Spectroscopy Upgrade for Nikon C1si (PicoQuant GmbH) microscope. The fluorescence-signal was detected through a 620 nm long-pass filter (Thorlabs Inc.) using a single-photon-counting avalanche photodiode (SPAD) (Micro Photon Devices) and counted by a time-correlated singlephoton counter PicoHarp 300 (PicoQuant GmbH). The resolution of FLIM images was 512×512 pixels.

Data analysis

Fluorescence decays were fitted using Edinburgh-F900 software package F900. For biexponential fluorescence decays, intensity-weighted lifetimes were calculated [Eq. (2)]:

$$\bar{\tau} = \frac{\sum_i a_i \tau_i^2}{\sum_i a_i \tau_i} \quad (2)$$

where a is an amplitude value and τ is the value of the lifetime. The goodness-of-fit parameter (χ^2) was 1.5 or less for single decays. Brightfield and fluorescence microscopy images were done using the Nikon EZ–C1 Bronze version 3.80 and ImageJ 1.52a software. FLIM image analysis was performed using the FLIMfit software tool developed at Imperial College London.[60] Further data processing and analysis were done with Origin 2018.

Acknowledgement

Quantum chemical computations were carried out using resources at the High-Performance Computing Center "HPC Saulėtekis" (Vilnius University, Faculty of Physics). This research was funded by a grant (no. S-MIP-19-6) from the Research Council of Lithuania.

Conflict of Interest

The authors declare no conflict of interest.

Keywords: Density functional calculations · Fluorescence spectroscopy · Molecular rotors · Viscosity sensing

[1] G. Deliconstantinos, V. Villiotou, J. C. Stavrides, *Biochem. Pharmacol.* **1995**, *49*, 1589–1600.
[2] O. Nadiv, M. Shinitzky, H. Manu, D. Hecht, C. T. Roberts, D. LeRoith, Y. Zick, *Biochem. J.* **1994**, *298*, 443–450.
[3] G. S. Zubenko, U. Kopp, T. Seto, L. L. Firestone, *Psychopharmacology* **1999**, *145*, 175–180.
[4] H. Xiao, P. Li, B. Tang, *Chem. A Eur. J.* **2020**.
[5] M. K. Kuimova, *Phys. Chem. Chem. Phys.* **2012**, *14*, 12671–12686.
[6] M. A. Haidekker, E. A. Theodorakis, *Org. Biomol. Chem.* **2007**, *5*, 1669–1678.
[7] A. Vyšniauskas, M. K. Kuimova, *Int. Rev. Phys. Chem.* **2018**, *37*, 259–285.
[8] D. Su, C. L. Teoh, L. Wang, X. Liu, Y. T. Chang, *Chem. Soc. Rev.* **2017**, *46*, 4833–4844.
[9] M. A. Haidekker, M. Nipper, A. Mustafic, D. Lichlyter, M. Dakanali, E. A. Theodorakis in *Adv. Fluoresc. Reporters Chem. Biol. I*, Springer, Berlin, Heidelberg, **2010**, pp. 267–308.
[10] S. C. Lee, J. Heo, H. C. Woo, J. A. Lee, Y. H. Seo, C. L. Lee, S. Kim, O. P. Kwon, *Chem. A Eur. J.* **2018**, *24*, 13706–13718.
[11] J. E. Chambers, M. Kubánková, R. G. Huber, I. López-Duarte, E. Avezov, P. J. Bond, S. J. Marciniak, M. K. Kuimova, *ACS Nano* **2018**, *12*, 4398–4407.
[12] M. K. Kuimova, G. Yahioglu, J. A. Levitt, K. Suhling, *J. Am. Chem. Soc.* **2008**, *130*, 6672–6673.
[13] I. E. Steinmark, A. L. James, P. H. Chung, P. E. Morton, M. Parsons, C. A. Dreiss, C. D. Lorenz, G. Yahioglu, K. Suhling, *PLoS One* **2019**, *14*, 1–20.
[14] A. Vyšniauskas, I. López-Duarte, N. Duchemin, T.-T. Vu, Y. Wu, E. M. Budynina, Y. A. Volkova, E. Peña Cabrera, D. E. Ramírez-Ornelas, M. K. Kuimova, *Phys. Chem. Chem. Phys.* **2017**, *19*, 25252–25259.
[15] A. S. Klymchenko, *Acc. Chem. Res.* **2017**, *50*, 366–375.
[16] A. Polita, S. Toliautas, R. Žvirblis, A. Vyšniauskas, *Phys. Chem. Chem. Phys.* **2020**, *22*, 8296–8303.
[17] W. Miao, C. Yu, E. Hao, L. Jiao, *Front. Chem.* **2019**, *7*, 1–6.
[18] M. Kubánková, I. López-Duarte, D. Kiryushko, M. K. Kuimova, *Soft Matter* **2018**, *14*, 9466–9474.
[19] M. Kubánková, P. A. Summers, I. López-Duarte, D. Kiryushko, M. K. Kuimova, *ACS Appl. Mater. Interfaces* **2019**, *11*, 36307–36315.
[20] I. López-Duarte, T. Truc Vu, M. A. Izquierdo, J. A. Bull, M. K. Kuimova, *Chem. Commun.* **2014**, *50*, 5282–5284.
[21] L. E. Shimolina, M. A. Izquierdo, I. López-Duarte, J. A. Bull, M. V. Shirmanova, L. G. Klapshina, E. V. Zagaynova, M. K. Kuimova, *Sci. Rep.* **2017**, *7*, 1–11.
[22] P. S. Sherin, I. López-Duarte, M. R. Dent, M. Kubánková, A. Vyšniauskas, J. A. Bull, E. S. Reshetnikova, A. S. Klymchenko, Y. P. Tsentalovich, M. K. Kuimova, *Chem. Sci.* **2017**, *8*, 3523–3528.
[23] M. Olšinová, P. Jurkiewicz, M. Pozník, R. Šachl, T. Prausová, M. Hof, V. Kozmík, F. Teplý, J. Svoboda, M. Cebecauer, *Phys. Chem. Chem. Phys.* **2014**, *16*, 10688–10697.
[24] M. R. Dent, I. López-Duarte, C. J. Dickson, N. D. Geoghegan, J. M. Cooper, I. R. Gould, R. Krams, J. A. Bull, N. J. Brooks, M. K. Kuimova, *Phys. Chem. Chem. Phys.* **2015**, *17*, 18393–18402.
[25] Y. Wu, M. Štefl, A. Olzyńska, M. Hof, G. Yahioglu, P. Yip, D. R. Casey, O. Ces, J. Humpolíčková, M. K. Kuimova, *Phys. Chem. Chem. Phys.* **2013**, *15*, 14986–14993.
[26] A. Vyšniauskas, M. Qurashi, M. K. Kuimova, *Chem. A Eur. J.* **2016**, *22*, 13210–13217.
[27] N. A. Hosny, G. Mohamedi, P. Rademeyer, J. Owen, Y. Wu, M. X. Tang, R. J. Eckersley, E. Stride, M. K. Kuimova, *Proc. Natl. Acad. Sci. USA* **2013**, *110*, 9225–9230.
[28] J. M. Nölle, C. Jüngst, A. Zumbusch, D. Wöll, *Polym. Chem.* **2014**, *5*, 2700–2703.
[29] N. A. Hosny, C. Fitzgerald, A. Vyšniauskas, A. Athanasiadis, T. Berkemeier, N. Uygur, U. Pöschl, M. Shiraiwa, M. Kalberer, F. D. Pope, M. K. Kuimova, *Chem. Sci.* **2016**, *7*, 1357–1367.
[30] J. A. Levitt, P. H. Chung, M. K. Kuimova, G. Yahioglu, Y. Wang, J. Qu, K. Suhling, *ChemPhysChem* **2011**, *12*, 662–672.
[31] R. Weissleder, *Nat. Biotechnol.* **2001**, *19*, 316–317.
[32] D. Zhang, V. Martín, I. García-Moreno, A. Costela, M. E. Pérez-Ojeda, Y. Xiao, *Phys. Chem. Chem. Phys.* **2011**, *13*, 13026–13033.
[33] J. R. Lakowicz, *Principles of Fluorescence Spectroscopy* 3rd ed., Springer, Boston, **2006**.
[34] V. J. Pansare, S. Hejazi, W. J. Faenza, R. K. Prud'Homme, *Chem. Mater.* **2012**, *24*, 812–827.
[35] Y. Ni, J. Wu, *Org. Biomol. Chem.* **2014**, *12*, 3774–3791.
[36] C. S. Kue, S. Y. Ng, S. H. Voon, A. Kamkaew, L. Y. Chung, L. V. Kiew, H. B. Lee, *Photochem. Photobiol. Sci.* **2018**, *17*, 1691–1708.
[37] E. Lager, J. Liu, A. Aguilar-Aguilar, B. Z. Tang, E. Peña-Cabrera, *J. Org. Chem.* **2009**, *74*, 2053–2058.

[38] X. Liu, W. Chi, Q. Qiao, S. V. Kokate, E. P. Cabrera, Z. Xu, X. Liu, Y.-T. Chang, *ACS Sens.* **2020**, *5*, 731–739.
[39] J. Cui, H. Nie, S. Zang, S. Su, M. Gao, J. Jing, X. Zhang, *Sens. Actuators B* **2021**, *331*, 129432.
[40] B. Le Guennic, D. Jacquemin, *Acc. Chem. Res.* **2015**, *48*, 530–537.
[41] R. Berraud-Pache, F. Neese, G. Bistoni, R. Izsák, *J. Chem. Theory Comput.* **2020**, *16*, 564–575.
[42] M. R. Momeni, A. Brown, *J. Chem. Theory Comput.* **2015**, *11*, 2619–2632.
[43] S. Toliautas, J. Dodonova, A. Žvirblis, I. Čiplys, A. Polita, A. Devižis, S. Tumkevičius, J. Šulskus, A. Vyšniauskas, *Chem. A Eur. J.* **2019**, *25*, 10342–10349.
[44] F. Li, S. I. Yang, Y. Ciringh, J. Seth, C. H. Martin, D. L. Singh, D. Kim, R. R. Birge, D. F. Bocian, D. Holten, J. S. Lindsey, *J. Am. Chem. Soc.* **1998**, *120*, 10001–10017.
[45] Q. Ou, Q. Peng, Z. Shuai, *J. Phys. Chem. Lett.* **2020**, *11*, 7790–7797.
[46] A. Prlj, L. Vannay, C. Corminboeuf, *Helv. Chim. Acta* **2017**, *100*, 1–9.
[47] Z. Lin, A. W. Kohn, T. Van Voorhis, *J. Phys. Chem. C* **2020**, *124*, 3925–3938.
[48] T. Suhina, S. Amirjalayer, S. Woutersen, D. Bonn, A. M. Brouwer, *Phys. Chem. Chem. Phys.* **2017**, *19*, 19998–20007.
[49] T. Förster, G. Hoffmann, *Zeitschrift für Phys. Chemie* **1971**, *75*, 63–76.
[50] K. P. Wall, R. Dillon, M. K. Knowles, *Biochem. Mol. Biol. Educ.* **2015**, *43*, 52–59.
[51] J. H. Brannon, D. Magde, *J. Phys. Chem.* **1978**, *82*, 705–709.
[52] R. G. Parr, *Density Functional Theory of Atoms and Molecules*, Oxford University Press, Oxford, **1989**.
[53] R. E. Stratmann, G. E. Scuseria, M. J. Frisch, *J. Chem. Phys.* **1998**, *109*, 8218–8224.
[54] Y. Zhao, D. G. Truhlar, *Theor. Chem. Acc.* **2008**, *120*, 215–241.
[55] R. A. Kendall, T. H. Dunning, R. J. Harrison, *J. Chem. Phys.* **1992**, *96*, 6796–6806.
[56] M. R. Momeni, A. Brown, *J. Phys. Chem. A* **2016**, *120*, 2550–2560.
[57] M. Cossi, N. Rega, G. Scalmani, V. Barone, *J. Comput. Chem.* **2003**, *24*, 669–681.
[58] M. J. Frisch, G. W. Trucks, H. B. Schlegel, G. E. Scuseria, M. A. Robb, J. R. Cheeseman, G. Scalmani, V. Barone, G. A. Petersson, H. Nakatsuji, X. Li, M. Caricato, A. V. Marenich, J. Bloino, B. G. Janesko, R. Gomperts, B. Mennucci, H. P. Hratchian, J. V. Ortiz, A. F. Izmaylov, J. L. Sonnenberg, D. Williams-Young, F. Ding, F. Lipparini, F. Egidi, J. Goings, B. Peng, A. Petrone, T. Henderson, D. Ranasinghe, V. G. Zakrzewski, J. Gao, N. Rega, G. Zheng, W. Liang, M. Hada, M. Ehara, K. Toyota, R. Fukuda, J. Hasegawa, M. Ishida, T. Nakajima, Y. Honda, O. Kitao, H. Nakai, T. Vreven, K. Throssell, J. A. Montgomery, Jr., J. E. Peralta, F. Ogliaro, M. J. Bearpark, J. J. Heyd, E. N. Brothers, K. N. Kudin, V. N. Staroverov, T. A. Keith, R. Kobayashi, J. Normand, K. Raghavachari, A. P. Rendell, J. C. Burant, S. S. Iyengar, J. Tomasi, M. Cossi, J. M. Millam, M. Klene, C. Adamo, R. Cammi, J. W. Ochterski, R. L. Martin, K. Morokuma, O. Farkas, J. B. Foresman, D. J. Fox, Gaussian09, Revision D.01, Gaussian, Inc., Wallingford CT, **2013**.
[59] Cold Spring Harbor Laboratory Press, *PBS (pH 7.4) recipe*, 2018.
[60] S. C. Warren, A. Margineanu, D. Alibhai, D. J. Kelly, C. Talbot, Y. Alexandrov, I. Munro, M. Katan, C. Dunsby, P. M. W. French, *PLoS One* **2013**, *8*, e70687.

Manuscript received: July 29, 2021
Accepted manuscript online: September 22, 2021
Version of record online: November 3, 2021

